Use of Hybrid torque+position controller towards more realistic movement profiles of neurally controlled devices

Pratik Y. Chhatbar[1*,2,3], Joseph T. Francis[2,3,4,5]

[1*]Current affiliation: Department of Neurosciences, Medical University of South Carolina, Charleston, SC;
[2]Department of Physiology and Pharmacology, [3]Graduate Program in Biomedical Engineering, [4]Graduate Program in Neurobiology and Behavior,
[5]The Robert Furchgott Center for Neural and Behavioral Science, SUNY Downstate Medical Center, Brooklyn, NY

Neuroscience 2011
84.25/RR19

Introduction

Technology of neural control of devices for movements currently lack user input on compliance of the device. With variety of compliance settings at various joints of the robotic arm, the user can best perform reaching and grasping movements. This will ensure robust control of intentional components of the movement, while allowing variations in the non-intentional components of the movement. We will address one possible way to address it with hybrid torque+position control of robotic movements.

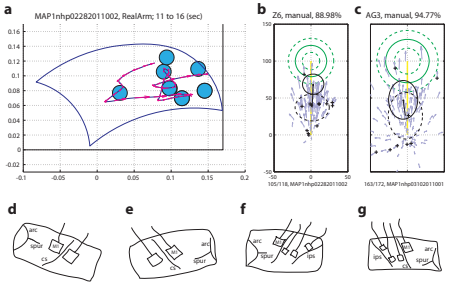

Fig 1: Task, FSPV plots and microelectrode array implant locations: *(a) random target pursuit (RTP) task during manual/BMI performance. (b,c) normalized first sub-movement peak velocity (FSPV) plots: Title shows animal ID, task type as manual and percent successful trials. Actual numbers of successful and total considered trials are presented in the bottom, next to the recorded file name. Further explanation can be found in the methods section. (d-k) Array placement for the two animals based on digital photographs taken at the time of surgery. Top of the figures always represent rostral/medial direction towards sagittal sulcus. Anterior is direction of junction of arcuate sulcus and its spur (arrow head) relative to central sulcus (arrow). (d) Z6 left and (e) right brain M1 and S1 (area 1-2) implant (96 channels) in shoulder representative region. Animal Z6 was implanted for the third time in left M1 and S1 regions at the same implant location. (f) AG3 left and (g) right brain implant in M1 (96 channels) shoulder representative region, S1 area 1, 2 hand representative regions and area PE (32 channels each).*

$$\hat{y}(T) = b + \sum_{i=1}^{m}\sum_{t=1}^{n}(a_i(t)\cdot S_i(T-t))$$

$$S_{(1xp)}(T) = N_{(1xp)}(T)\, Q_{(pxp)}$$

$$\vec{\tau}_{mon} = M(\theta)\ddot{\theta} + C(\theta,\dot{\theta})\dot{\theta} + G(\theta) - \vec{\tau}_{cmd} - \vec{\tau}_{frc}$$

$$\Theta_{plant}(t) = (1-\alpha)\left(\widehat{\Theta_{tor}(t)}\right) + \alpha(\widehat{\Theta_{pos}(t)})$$

Reprint requests: chhatbar@musc.edu

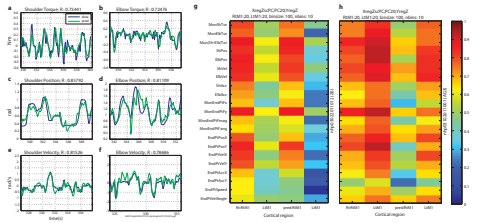

Fig 2: Open loop performance of the decoder: *(a-f) Sample plot of prediction values (green) overlaid on actually recorded or calculated joint torques, positions and velocities during manual task. R-values are shown along with the respective parameter in the title of the subplot. About 10 seconds of data is shown for each parameter. Predictions are made on a new dataset using coefficients calculated by multiple linear regression of first 20 principal components of all units recorded from M1 (ipsilateral, in this case, on monkey Z6) against the behavioral parameter from different dataset Data was binned at 100 ms and past 10 bins were used for predictions. (g-h) summary R-value plots of fits (estimates on same dataset, left 2 columns) and predictions (estimates on new dataset, right 2 columns) on multiple behavioral variables using first 20 principal components. (g) Z6 and (h) AG3. Acronym key: fit = fit values, pred = prediction values, Rt = Right side, M1 = primary motor cortex, shoulder-representative region; Mon = monkey generated, Sh = shoulder, Elb = elbow, Tor = torque, Pos = position, Vel = velocity, Acc = acceleration, EndPt = End-point/end-effector - about the tip of middle finger of the monkey, F = force, x = X-direction, y = y-direction, mag = magnitude, ang = angle.*

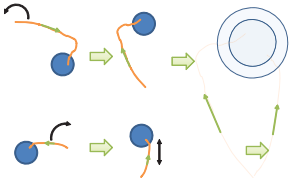

Fig 3: FSVP: *Example movements and their inclusion in first sub-movement velocity plot (FSVP) after generalization by rotation and/or scaling*

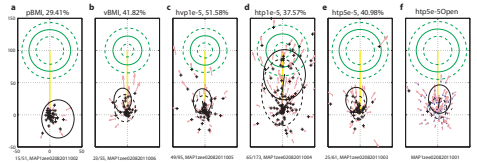

Fig 4: Effect of position prediction influence on the first sub-movement peak-velocity (FSPV) under variety of closed-loop BMI controllers on a single day *(loop is closed by vision of the workspace), animal Z6. (a) position BMI (pBMI) (b) velocity BMI (vBMI) (c) hybrid velocity-position BMI, 0.001% position influence (hvp1e-5) (d) hybrid torque-position BMI, 0.001% position influence (htp1e-5) (e) hybrid torque-position BMI, 0.005% position influence (htp5e-5) (f)open-loop htp5e-5 (htp5e-5Open) without animal's knowledge while doing manual task.*

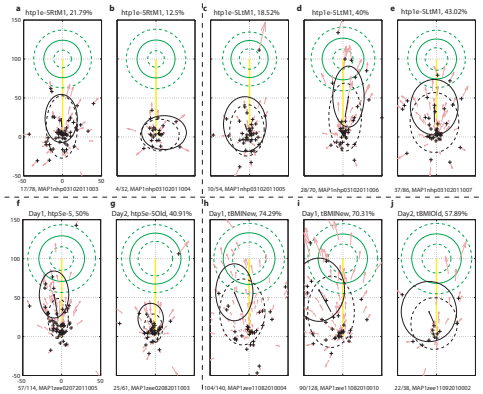

Fig 5: Changes in the performance with continued usage of BMI over time. *(a-e) animal AG3: (a,b) using ipsilateral M1 hybrid torque-position BMI with 0.001% position influence (htp1e-5RtM1). (c,d,e) using contralateral M1 (htp1e-5LtM1). (f-j) animal Z6 across days: (f,g) htp5e-5 controller with set of coefficients across the day led to slightly decreased success rate, more constricted FSPV distribution and directionality ($p<0.05$) but similar mean FSPV direction ($p>0.1$). (h,i) Using pure torque controller (tBMI) with fresh coefficients from same day manual task (j) using same decoder from previous day led to no significant difference in mean FSPV direction ($p>0.1$, Kuiper test).*

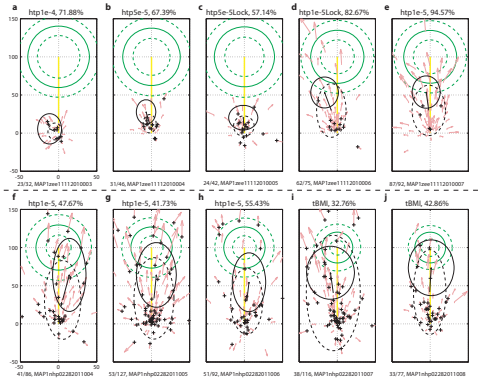

Fig 6: Effect of position influence in hybrid torque-position BMI: *(top row) decreasing position influence from 0.01% (a) to 0.005% (b-c) to 0.001% (d-e). Real arm was locked in (c,d) at 75° shoulder and 85° elbow. (bottom row, f-j) Decreasing position influence from 0.001% to 0% (pure torque control). The real arm was locked at the center of the workspace, at 25° shoulder and 85° elbow.*

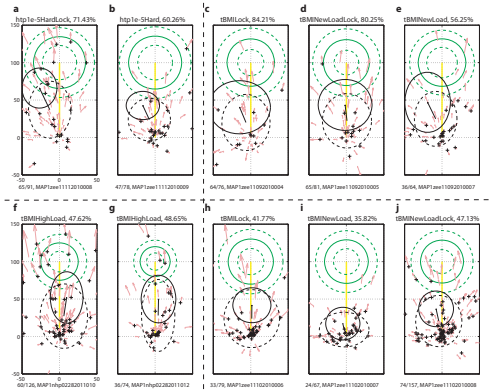

Fig 7: Adaptation through novel task conditions: *(a,b – htp1e-5) Increased task difficulty led to faster movements and decreased success-rate (a, compare with Figure 4.5,d-e). followed by slowing down by the animal (b, decrease in FSPV distribution and directionality). (f-g, tBMI) Increased viscous gain-fields (joint-angular velocity-dependent resistive torques, equal versus high, see Table 4 2) led to slower movements and improved the success-rate ($p<0.05$, g, compare with Figure 4.5,i,j). (c-e; h-j tBMI) Introduction of novel viscous gain-fields inside the bounds of ongoing low- and high- gain fields (routine versus novel, see Table 4 2), no significant difference in FSPV distribution or directionality found even under freely moving actual arm versus locked arm (75,85 degrees) configurations.*

Conclusion & Future Directions

Our results suggest that simple mathematical approach combined with inertial dynamics of the system can provide real-time neural control of joint torques. More experiments are required to test the long-term performance and adaptation rates of the decoder to novel external dynamic environments, with/out proprioceptive feedback. All in all, hybrid torque-position BMI with neural control of influence of each component (torque and position) might play a crucial role in sensorimotor neuroprostheses. This way, neural control of 'impedence' at each individual degree of freedom of the prosthetic device can be achieved. This will bring us closer to the ultimate goal of majority of the dexterous movements - reaching and grasping.

Select References

a) Towards implementing impedance control in sensorimotor neuroprostheses. P. Y. Chhatbar Doctoral Thesis submitted to SUNY Downstate Medical Center, Brooklyn, NY, May 2011.
b) Serruya, M. D., N. G. Hatsopoulos, et al. (2002). "Instant neural control of a movement signal." Nature 416(6877): 141-142.
c) Velliste, M., S. Perel, et al. (2008). "Cortical control of a prosthetic arm for self-feeding." Nature 453(7198): 1098-1101.
d) O'Doherty, J. E., M. A. Lebedev, et al. (2011). "Active tactile exploration using a brain-machine-brain interface." Nature doi:10.1038/nature10489.
e) Ganguly, K., L. Secundo, et al. (2009). "Cortical representation of ipsilateral arm movements in monkey and man." J Neurosci 29(41): 12948-12956.

This work is supported by NYS Department of Health SCIRBs # C022048, DARPA REPAIR Contract# N66001-10-C-2008 and SUNY Downstate Medical School.